Clustering behavior during natural aging and artificial aging in Al-Mg-Si alloys with different Ag and Cu addition

Clustering behavior during natural aging and artificial aging in Al-Mg-Si alloys with different Ag and Cu addition

Yaoyao Weng, Zhihong Jia, Lipeng Ding, Shiji Muraishi, Qing Liu

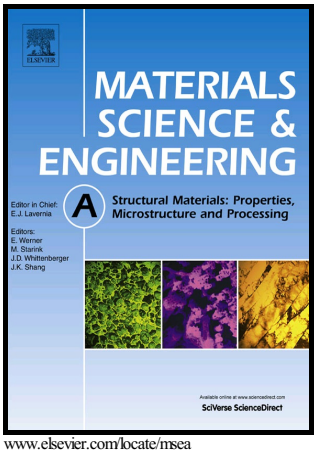

www.elsevier.com/locate/msea

PII: S0921-5093(18)30943-2
DOI: https://doi.org/10.1016/j.msea.2018.07.018
Reference: MSA36682

To appear in: *Materials Science & Engineering A*

Received date: 26 April 2018
Revised date: 5 July 2018
Accepted date: 6 July 2018

Cite this article as: Yaoyao Weng, Zhihong Jia, Lipeng Ding, Shiji Muraishi and Qing Liu, Clustering behavior during natural aging and artificial aging in Al-Mg-Si alloys with different Ag and Cu addition, *Materials Science & Engineering A,* https://doi.org/10.1016/j.msea.2018.07.018

Clustering behavior during natural aging and artificial aging in Al-Mg-Si alloys with different Ag and Cu addition

Yaoyao Weng[a,e], Zhihong Jia[a,b,*], Lipeng Ding[c,d], Shiji Muraishi[e], Qing Liu[a]

[a]*International Joint laboratory for Light Alloys (Ministry of Education), College of Materials Science and Engineering, Chongqing University, Chongqing 400044, China*

[b]*Electron Microscopy Center of Chongqing University, Chongqing 400044, China*

[c]*Université catholique de Louvain, Institute of Mechanics, Materials and Civil Engineering, IMAP, 1348 Louvain-la-Neuve, Belgium*

[d]*Electron Microscopy for Materials Science (EMAT), Department of Physics, University of Antwerp, Groenenborgerlaan 171, B-2020 Antwerp, Belgium*

[e]*Department of Materials Science and Engineering, Tokyo Institute of Technology, 2-12-1-S8-5 Ookayama, Meguro-ku, Tokyo 152-8552, Japan*

Abstract:

The effect of Ag and Cu addition on clustering behavior of Al-Mg-Si alloys during natural aging (NA) and artificial aging (AA) was investigated by hardness measurement, tensile test and atom probe tomography analysis. The results show that both Ag and Cu atoms could enter clusters and GP-zones, change the Mg/Si ratio and increase their volume fractions. Compared with the A1 base alloy, the clusters in the Ag/Cu-added alloys more easily transform to β″ phases for size and compositional similarity, and the strengthening ability of these particles is enhanced by the increased volume fraction and shear modulus. In NA condition, Cu is greater in improving the volume fraction of clusters than Ag and thus produces higher T4 temper hardness. In AA condition, in contrary, Ag is more effective in facilitating the formation and growth of particles than Cu due to the stronger Ag-Mg interaction and the high diffusivity of Ag atoms in Al matrix, leading to highest hardening response. Compared to the Cu-added alloy, the Ag-added alloy shows higher precipitation kinetics during AA treatment and maintains a lower T4 temper hardness.

Keywords: Al-Mg-Si alloys; Ag addition; Cu addition; Clustering behavior; Atom probe tomography;

1. Introduction

Heat-treatable Al-Mg-Si (6xxx) alloys are widely used as body-sheet materials for automobile because of their excellent combined performance of high strength, good formability and corrosion resistance [1]. These alloys are strengthened by the nano-sized metastable precipitates during aging treatment [2]. For automobile application, the aluminium sheets are inevitably stored for a period at room temperature (RT) for transportation and stamped

into car parts in car factories. After that, these sheets undergo the bake hardening process at a high temperature (~453 K), and highly dense clusters and precipitates are formed that are responsible for the increased strength. To satisfy the required in-service dent resistance, alloy sheets should have low strength during stamping and high strength after paint bake (PB) treatment [3]. Atomic clusters formed in natural aging (NA) and early stage of artificial aging (AA) need to be fully understood to increase the properties of these alloys. The reason why clusters formed in the early precipitation stage so important is due to: (1) a relatively low temperature and short duration of the commercial PB cycle (typically at 443 – 453 K for 20 – 30 min) applied by industry could not reach the full precipitation of β″ with maximum hardness, thus the strength of alloys actually depends on the clusters and precipitates formed in the early stage of aging; (2) the clusters formed during NA could not only decrease the formability of T4 temper, but also retard the precipitation of β″ during PB cycle, resulting in a poor dent resistance; (3) knowledge about clusters in the early stage of aging is essential for developing new heat treatment process, such as pre-aging treatment [4].

Detailed studies have attempted to analyze the clusters formed during NA and early stage of AA by various experimental techniques, such as differential scanning calorimetry (DSC), electrical resistivity, positron annihilation spectroscopy and atom probe tomography (APT). A. Serizawa et al. [5] reported two types of nanoclusters, Cluster(1) and Cluster(2), are formed at RT and 373 K in Al-Mg-Si alloys, respectively. Cluster(1) has the wide range of Mg/Si ratio and can't transform to β″ precipitate, while Cluster(2) can transform continuously into β″ for size and compositional similarity. Using the low-temperature DSC, C.S.T. Chang et al. [6] revealed that three clustering reactions take place during NA. The first two reactions are linked to each other and completed after 1 hour, corresponding to the formation of Si-rich clusters. The third reaction stems from Mg slowly diffusing to these clusters for at least 1 week, eventually forming Mg-Si co-clusters. G.A. Edwards et al. [2] found direct evidence for the separate Si-clusters, Mg-clusters and Mg-Si co-clusters during aging at 343 K using the atom probe field ion microscope (APFIM) technique. They proposed that the initial clustering sequence is as follow: Al SSS → clusters of Si atoms and clusters of Mg atoms → dissolution of Mg-clusters → formation of Mg-Si co-clusters. Besides, they considered that the nature of clusters (i.e. co-cluster or individual cluster, Mg/Si ratio), rather than their size, is critical for the ability of clusters to act as nuclei for subsequent precipitates. V. Fallah [7] suggested that, regardless of NA or AA treatment, the earliest clusters are Si-rich and gradually undergo a simultaneous coarsening and Mg-enrichment process upon increasing the aging time. Only AA clusters can reach the composition level required for stabilization, while the NA clusters do not become stabilized within the

achievable simulation times. However, due to the small size and highly coherent of clusters, understanding on clusters is still inadequately, especially the relationship between the composition and clusters evolution during different aging conditions.

Cu and Ag are the two important elements often added in Al-Mg-Si alloys to improve their properties. Both Cu and Ag can significantly increase precipitation kinetics and age hardening response of these alloys [8-10]. Our previous work showed that Ag addition can produce a lower NA hardness and higher PB hardening response compared with Cu [11]. Till now, the influence mechanism of Cu/Ag on precipitation has been extensively studied, however, the influence of Cu/Ag on the clustering behavior of Al-Mg-Si alloys is less studied. In view of the dominant role of clusters in determining the precipitation kinetics of Al-Mg-Si alloys, revealing the clustering mechanism for the Ag/Cu-added Al-Mg-Si alloys is of significantly implication. Besides, understanding the relationship between Ag/Cu addition and clusters evolution can shed light on the novel alloy design. In the present study, hardness measurement, tensile test and APT analysis were used to investigate the clustering behavior for Al-Mg-Si alloys with different Ag and Cu addition both in T4 temper and AA condition. The clustering mechanism for these alloys was explored and the strengthening ability of clusters was studied by yield stress modelling.

2. Experimental

Table 1 shows the chemical compositions of the four investigated Al-Mg-Si alloys. The concentrations of Ag and Cu for these alloys were varied (A2: 0.12 at % Ag, A3: 0.07 at % Ag and 0.10 at % Cu, A4: 0.21 at % Cu). The as-cast alloys were homogenized, hot and cold rolled to 1.0 mm thick sheets. Samples were solution heat treated in a muffle furnace at 843 K for 20 min and water quenched to RT. Two types of aging treatments were applied immediately after water quenching (WQ) to investigate the clustering behavior for Al-Mg-Si alloys, (1) NA at RT for 2 weeks, (2) AA at 443 K were performed in oil baths, and the samples artificially aged at 443 K for 5 min were selected to study the clustering behavior.

Vickers microhardness was measured at RT using a MH-5L microhardness tester with a load of 500g and a dwell time of 10s. The error in Vickers hardness was less than ±3%. The tensile properties of the sheet samples were measured by an SHIMADZUAG-X10KN computer controlled test machine. The samples with 25 mm gauge length were stretched along the rolling direction with a tensile rate of 2 mm/min. For each condition, three parallel specimens were tested in order to verify the experimental results. The atom probe analysis was carried out using a

CAMECA LEAP4000HR instrument with a voltage pulse repetition rate of 200 kHz, pulse fraction (the ratio of pulse voltage to DC standing voltage) of 20% and specimen temperature of 25 K. The analysis of the 3DAP data was carried out using IVAS^{TM} 3.6.8 software. A separation distance (d_{max}) of 0.5 nm and N_{min} of 10 solute atoms was used. As N_{min} was set at 10, particles containing fewer than 10 detected solute atoms were not selected. The equivalent radius (R) of particles is calculated by the equation: $R = (3n\Omega/4\pi f)^{1/3}$, n is the atomic number of particles, Ω, the atomic volume, is 1.66×10^{-2} nm^3 for aluminum, and *f* is detector efficiency. The number density of particles (N_V) is usually described by the equation: $N_V = (N_p\times f)/(n_a\times\Omega)$, N_p is the number of particles in bulk volume, and n_a is the total atomic number in bulk volume. A detector efficiency of 36% was considered in calculating the number density of clusters.

3. Results

3.1. Hardness and tensile measurements

The hardness values for the four alloys after 2 weeks of NA are shown in Fig. 1(a). The Ag/Cu-added alloys had higher T4 temper hardness than the A1 base alloy, particularly the Cu-added A4 alloy. It is suggested that Ag and Cu could increase the hardening potential of Al-Mg-Si alloy after RT storage for 2 weeks. Fig. 1(b) shows the hardness values for the four alloys after AA at 443 K for 5 min and 30 min. The hardness response was increased with the AA time prolonged. Compared with the A1 base alloy, the Ag/Cu-added alloys had overall higher hardness after aging at 443 K for 5 min and 30 min. It is evident that Ag and Cu could improve the precipitation hardening response for Al-Mg-Si alloys during AA treatment. Different from NA condition, the Ag-added A2 alloy had higher AA hardening response than the Cu-added A4 alloy, implying that Ag is stronger in facilitating the precipitation for these alloys than Cu.

The yield strength (YS), ultimate tensile strength (UTS) and elongation of the four alloys after NA for 2 weeks and AA at 443K for 5min are listed in Table 2. Both YS and UTS after NA and AA treatments were increased with Ag and/or Cu additions, which are in agreement with the hardness results shown in Fig. 1. The Cu-added A4 alloy had the highest YS (186.84 MPa) in T4 temper and a slight lower YS (185.48 MPa) after AA at 443K for 5min. In contrary, the Ag-added A2 alloy had a relatively lower YS (163.44 MPa) in T4 temper and highest YS (210.84 MPa) after AA for 5min, which is an expected variation of properties for automobile application. The Cu-Ag-added A3 alloy had a higher YS (177.98 MPa) in T4 temper and YS (205.31 MPa) after

AA for 5min. Compared with the A1 base alloy, the elongation of the Ag/Cu-added alloys was decreased, and similar elongation were presented for the three Ag/Cu-added alloys.

3.2. APT analysis

3.2.1. Natural aging for two weeks

APT elemental maps of solute atoms for the four alloys after 2 weeks NA are shown in Fig. 2. The Mg, Si, Ag and Cu atoms are depicted as purple, blue, red and orange spheres, respectively, while the Al atoms are not displayed in order to clearly elucidate the clusters. The number density of clusters as a function of the cluster size for the four alloys are shown in Fig. 3. It is obvious that all the clusters had the size below 1.0 nm. For the A1 base alloy, most of clusters had the size smaller than 0.6 nm. The cluster size was increased after Ag and/or Cu additions, implying that Ag and Cu could promote the growth of clusters after a long time NA treatment. The total number density of clusters were measured as $13.81\times10^{22}/m^3$, $6.19\times10^{22}/m^3$, $12.41\times10^{22}/m^3$ and $13.95\times10^{22}/m^3$ for the A1, A2, A3 and A4 alloys in T4 temper, respectively. It could be seen that the Ag-added A2 alloy had the lowest number density of clusters, while the number density of clusters for A1, A3 and A4 alloys were quite similar.

The distributions of the detected Mg/Si ratio of clusters as a function of the cluster size after 2 weeks NA for the four alloys are plotted in Fig. 4. The Mg/Si ratio of clusters for the four alloys were rather dispersive in T4 temper, which varied in a range of 0 and 5.0. No relationship between Mg/Si ratio and cluster size was found. The average Mg/Si ratio, (Mg + X)/Si ratio and X/Mg ratio of clusters for the four alloys after 2 weeks NA are listed in Table 3. X represents for Ag, Ag + Cu and Cu for the A2, A3 and A4 alloys, respectively. The average Mg/Si ratio of clusters were measured as 1.89, 1.83, 1.48 and 1.34 for the A1, A2, A3 and A4 alloys, respectively. The average Mg/Si ratio of clusters was decreased with addition of Cu, while Ag had no evident influence. The (Mg + X)/Si ratio of clusters was larger than the Mg/Si ratio for the Ag/Cu-added alloys, implying the incorporation of Ag and Cu atoms into clusters. The distributions of X/Mg ratio as a function of the cluster size for the three Ag/Cu-added alloys after 2 weeks NA are plotted in Fig. 5. The X/Mg ratio of clusters were rather small, varying between 0 and 0.6. It indicated that the incorporation of Ag and Cu atoms into clusters is rather weak in RT. The Mg-Si-X co-clusters coexisted with Mg-Si co-clusters in Al matrix for the three Ag/Cu-added alloys. The distribution of the measured X/Mg ratio became narrower as cluster size increased (remaining between 0 and 0.2),

suggested that Ag and Cu contents are more stable in the large clusters.

3.2.2. Early stage of artificial aging

APT elemental maps of solute atoms for the four alloys after AA at 443K for 5 min are shown in Fig. 6. Compared with the NA condition, the number density and size of particles for the four alloys were significantly increased in AA condition. The number density of particles as a function of the particle size for the four alloys are shown in Fig. 7. The Ag/Cu-added alloys had higher number density and larger particle size than that of the A1 base alloy, and the Ag-added A2 alloy had the highest number density of particles. It is suggested that Ag and Cu could facilitate the nucleation and growth of particles for Al-Mg-Si alloys, particularly Ag.

The relationship between Mg/Si ratio and particle size for the four alloys after AA for 5 min are plotted in Fig. 8. It could be seen that the distribution of Mg/Si ratio of particles was rather dispersive at a smaller particle size, but tended to narrow with increasing the size. Compared with the A1 base alloy, the Ag/Cu-added alloys had narrower Mg/Si ratio distribution as the particle size increased, especially the Ag-added A2 alloy and the Ag-Cu-added A3 alloy. Obtaining a simple criteria to judge the cluster or GP zone is always challenging under current characterization techniques, because they are so small and also can be affected by many factors, such as composition, heat treatment conditions etc [12-14]. In this work, based on the distribution law in Fig. 8 and the HAADF-STEM images of GP zones (Fig. S1 in supplementary materials), the particles smaller than 1 nm in radius are denoted as clusters, and those particles larger than 1 nm are labelled as GP-zones. Both clusters and GP zones are formed in the four alloys with majority of clusters after AA at 443K for 5 min. The percentages of GP-zones were 3%, 13%, 11% and 7% for the A1, A2, A3 and A4 alloys (as shown in Fig. 7), respectively, implying that Ag and Cu could obviously accelerate the transition of clusters to GP-zones. The average Mg/Si ratio, (Mg + X)/Si ratio and X/Mg ratio of clusters and GP-zones for the four alloys after 5 min AA treatment at 443 K are listed in Table 4. All the four alloys had similar average Mg/Si ratio for clusters (1.6 – 1.7), implying that Ag and Cu have no influence on the average Mg/Si ratio of clusters. While for GP zones, it is obvious that the Ag/Cu-added alloys had smaller average Mg/Si ratio, with the value similar to that of clusters, indicating that Ag and Cu could accelerate the transition of clusters to GP zones. For both clusters and GP-zones, the average (Mg + X)/Si ratio was larger than the average Mg/Si ratio, implying the incorporation of Ag and Cu atoms into clusters and GP zones. Similar average X/Mg ratio for GP zones was presented in the three Ag/Cu-added alloys, implying that similar amount of Ag and Cu are incorporated into GP zones. The distributions of X/Mg ratio as a

function of the particle size for the three Ag/Cu-added alloys after AA at 443K for 5 min are plotted in Fig. 9. Compared with NA condition, the X/Mg ratio of particles formed after AA was rather larger, varying between 0 and 1.0, indicating that the incorporation of Ag and Cu atoms into particles becomes stronger at 443 K. Similar to that of Mg/Si ratio, the X/Mg ratio for the small particles had a dispersive distribution. While the X/Mg ratio of GP zones showed a narrow value between 0 and 0.2, implying stable contents of Ag and Cu within the GP zones.

4. Yield stress calculation

Apparently, cluster hardening is an indispensable strengthening mechanism during the early stage of aging for Al-Mg-Si alloys. The macroscopic yield stress of particles could be calculated by a recently developed areal glide model [15] using the output from the atom probe analysis. The strength of particles is assumed to be chemistry independent and each set of particles is assumed to be spherical in shape with their radii, and the particles both in AA and NA are fine and sheared by dislocations. The contribution of clusters to yield strength is obtained from the recent calculation of R.K.W. Marceau et al. [16].

$$\sigma_{particle} = \mathrm{M}\frac{2\mathrm{T}}{bL_s^{cluster}}\tau^*_{cluster}$$

M is Taylor factor (assumed to be 3.06), and b is the Burgers vector. $L_s^{cluster}$ is an average spacing of spherical clusters, $\tau^*_{clusters}$ is a shear stress component and T is the line tension and taken as $0.5\mu_{cl}b^2$. The shear modulus of co-clusters, μ_{cl}, is commonly determined as a weighted average of the modulus of the individual pure substances [17, 18]. For a co-cluster as $Al_mMg_aSi_bAg_cCu_d$:

$$\mu_{cl} = \frac{\mathrm{m}\mu_{Al} + \mathrm{a}\mu_{Mg} + \mathrm{b}\mu_{Si} + \mathrm{c}\mu_{Ag} + \mathrm{d}\mu_{Cu}}{\mathrm{m} + \mathrm{a} + \mathrm{b} + \mathrm{c} + \mathrm{d}}$$

Following A.J. Ardell [19], the average spacing of spherical clusters ($L_s^{cluster}$) on the glide plane can be determined as:

$$L_s^{cluster} = \left(\frac{2\pi}{3f_{tot}}\right)^{1/2}\langle r_g\rangle$$

and the normalized shear stress component is:

$$\tau^*_{clusters} = 0.9\cos^{3/2}\frac{\varphi_{cluster}}{2}\left(1 - \frac{\cos^5\frac{\varphi_{cluster}}{2}}{6}\right)$$

where $<r_g>$ is the average particle radius and f_{tot} is the total volume fraction of clusters determined from the analysis of the atom probe data. $\varphi_{clusters}$ is the average breaking angle for the clusters, which in the range of 165~168^o [16].

The factors responsible to yield stress of particles for the four alloys after 2 weeks NA and 5 min AA are given in Table 5 and Table 6, respectively. Compared with the A1 base alloy, the particles in the three Ag/Cu-added alloys had higher shear modulus in both NA and AA conditions due to the entrance of larger shear modulus atoms, i.e. Ag and Cu (μ_{Cu} = 48.3 GPa, μ_{Ag} =30.3 GPa, μ_{Al} = 26.2 GPa, μ_{Mg} = 17.3 GPa [20, 21]). Notably, the volume fraction of particles is the dominant factor responsible to yield stress. Ag and/or Cu additions could facilitate the nucleation and growth of clusters, and thus the three Ag/Cu-added alloys had higher volume fraction of particles after NA and AA treatments. The difference is, in AA condition, the Ag-added A2 alloy had the highest volume fraction of particles. While in NA condition, the Cu-added A4 alloy had the highest volume fraction of particles. Besides, the average particle radius was increased after Ag and/or Cu additions in both AA and NA conditions.

The calculated yield stress ($\sigma_{particle}$) of particles by modulus hardening for the four alloys are listed in Table 7. The predicted $\sigma_{particle}$ of particles for the four alloys were lower than the experimental strength results listed in Table 2. It is because the yield stress of an alloy is a sum of base strength arising from the grain size (σ_0), solid-solution contribution (σ_{ss}) and particle contribution ($\sigma_{particle}$) [16]. The total $\sigma_{particle}$ of particles for the four alloys showed a similar tendency as the hardness and strength responses in both NA and AA conditions. In NA condition, although the number density of clusters in the Ag-added A2 alloy was lower than that of the A1 base alloy, the $\sigma_{particle}$ of A2 alloy was slightly higher than that of A1 alloy due to its higher volume fraction. The highest $\sigma_{particle}$ of Cu-added A4 alloy is mainly due to the high volume fraction and shear modulus of clusters. In AA condition, $\sigma_{particle}$ of the three Ag/Cu-added alloys were higher than that of the A1 base alloy, and the $\sigma_{particle}$ of the Ag-added A2 alloy was higher than that of the Cu-added A4 alloy. These results suggest that Ag and/or Cu additions could improve the strengthening ability of particles.

5. Discussion

From the APT analysis of these alloys, it is evident that both Ag and Cu could enter clusters and facilitate the nucleation and growth of clusters during NA and AA treatments. It is known that clustering behavior involves a complex interaction between vacancies and solute atoms. A high density of quench-in vacancy is formed

immediately after WQ and they can quickly be trapped by solute atoms to form clusters. The clusters formed in Al-Mg-Si alloys are mainly determined by the following three factors: interaction between various solute atoms, interaction between solute atoms and vacancy [22, 23], diffusion rate of solute atoms [24]. The impurity diffusion coefficient in solid is usually described by the Arrhenius equation: $D = D_0 exp\left[\frac{-Q}{RT}\right]$, where D_0 is denoted as the pre-exponential factor and Q as the activation energy. T denotes the absolute temperature and R is the gas constant [24]. The diffusion data and diffusion coefficient D for solute atoms at 293 K and 443 K in Al matrix are listed in Table 8. It is obvious that the diffusion coefficient of various solute atoms at 443 K is higher than that of 293 K. Ag has highest diffusion coefficient regardless of 443 K or 293 K, while the diffusion coefficient of Cu is rather small. Chemical interaction energies between various elements in Al matrix (eV + favored, - repulsive) taken from reference [23] are listed in Table 9. It could be seen that the interaction energy between Ag and vacancy is much higher than that of other solute atoms. Both Ag and Cu have a strong interaction energy with Mg, particularly Ag.

During NA treatment, as it is known that the clustering in Al-Mg-Si alloys mainly contains the formation of Si-clusters and Mg-clusters, dissolution of Mg-clusters and formation of Mg-Si co-clusters. After addition of Ag/Cu atoms, these atoms can incorporate into the Mg-Si co-clusters to form the Mg-Si-Ag/Cu co-clusters due to the strong interaction between Ag/Cu atoms and Mg atoms. It had been reported that the Cu atoms could increase the free energy level of quenching clusters, and thus promote the formation of clusters after long period NA. The increased free energy of clusters may be related to the effect of atomic size difference and the resultant elastic strain energy. The radius of Mg atom in solid solution is ~12% larger than Al atom, while Si and Cu atoms are ~6% and ~15% smaller than Al atom, respectively [13]. Incorporation of Cu atoms into the clusters minimizes the strain energy caused by the difference in atomic sizes, and thus makes the clusters more stable. The presence of Cu in clusters means that fewer vacancies are necessary to reduce the total strain energy of clusters, making clusters less efficient vacancy traps. Thus, the freedom vacancy in Al matrix is increased. As a result, the migration of solute atoms to clusters is easier in the Cu-added A4 alloy, thereby promoting the formation and growth of clusters. For the Ag-added A2 alloy, as the radius of Ag atom is similar to Al atom, which is not effective in reducing strain energy of clusters compared with Cu atom. Therefore, the facilitation of Ag on cluster's nucleation and growth is weak than that of Cu, leading to a lower hardness for the Ag-added A2 alloy in T4 temper. Due to the low diffusion coefficient of solute atoms at RT, the growth of clusters was relatively restricted and the cluster size was smaller than that of AA condition. The schematic illustrations of clusters evolution in the A1 base alloy, the Ag-added A2 alloy and the Cu-added A4 alloy during NA are shown in Fig. 10.

During AA treatment, for the three Ag/Cu-added alloys, the strong interaction between Ag/Cu and Mg can lead to the incorporation of Ag/Cu atoms into Mg-Si co-clusters, and Ag/Cu atoms can "steal" some Mg atoms from Mg-Si co-clusters to form the Ag/Cu-rich clusters and thus refine these clusters. Ag/Cu atoms actually act as the "dispersant", which increases the number density of clusters during initial stages of AA. Owing to the rather high diffusion coefficient of solute atoms during AA treatment, the long-range diffusion of various solute atoms occurred and the formation and growth of clusters are relatively easy. As Ag has higher diffusion coefficient and stronger interaction energy with vacancy and Mg, the refining effect of Ag on the clusters distribution is greater than that of Cu. Therefore, the number density and volume fraction of clusters in the Ag-added A2 alloy are higher than that of the Cu-added A4 alloy. The schematic illustrations of cluster evolution in the A1, A2 and A4 alloys during AA are shown in Fig. 11. The Ag-Cu-added A3 alloy has a slightly smaller number density of clusters than that of the Ag-added A2 alloy because the contents of Ag and Cu atoms are half of the A2 and A4 alloys. The improved volume fraction and shear modulus of particles for the three Ag/Cu-added alloys lead to higher strengthening ability of particles than that of the A1 base alloy.

6. Conclusions

Ag and Cu could participate in the nucleation and growth of clusters and increase the hardness and strength of Al-Mg-Si alloys during NA and AA treatments. Both Ag and Cu atoms could enter clusters and GP-zones, change the Mg/Si ratio and increase their volume fractions. Compared with the A1 base alloy, the clusters in the Ag/Cu-added alloys more easily transform to β″ phases for size and compositional similarity, and the strengthening ability of these particles is enhanced by the increased volume fraction and shear modulus.

The effect of Ag and Cu addition on clustering mechanism was different in NA and AA treatment. In NA condition, the Cu-added A4 alloy had higher T4 temper strength compared with the Ag-added A2 alloy owing to the improved number density and volume fraction of clusters. In AA condition, the Ag-added A2 alloy had higher strength than the Cu-added A4 alloy. It is due to Ag and Cu atoms easily enter clusters and facilitate the formation of clusters due to the strong interaction between Ag/Cu and Mg, and the volume fraction of particles in the Ag-added A2 alloy is further improved for the high diffusion rate of Ag.

Acknowledgments

This work was supported by the Special major R & D Projects for Key Technology Innovation of Key Industries in Chongqing (Grant No. cstc2017zdcy-zdzxX0006), the Fundamental Research Funds for the Central Universities of China (Grant No. 106112016CDJXZ338825 and 106112017CDJQJ308822) and the program of China Scholarships Council (No. 201706050125).

References

[1] W.S. Millera, L. Zhuanga, J. Bottemaa, A.J. Wittebrooda, P.D. Smetb, A. Haszlerc, A. Viereggec, Recent development in aluminium alloys for the automotive industry, Mater. Sci. Eng. A, 280 (2000) 37-49.

[2] G.A. Edwards, K. Stille, G.L. Dunlop, M.J. Couper, The precipitation sequence in Al-Mg-Si alloys, Acta Mater. 46 (1998) 3893-3904.

[3] M.A. van Huis, J.H. Chen, M.H.F. Sluiter, H.W. Zandbergen, Phase stability and structural features of matrix-embedded hardening precipitates in Al–Mg–Si alloys in the early stages of evolution, Acta Mater. 55 (2007) 2183-2199.

[4] Y. Birol, Pre-aging to improve bake hardening in a twin-roll cast Al–Mg–Si alloy, Mater. Sci. Eng. A, 391 (2005) 175-180.

[5] A. Serizawa, S. Hirosawa, T. Sato, Three-Dimensional Atom Probe Characterization of Nanoclusters Responsible for Multistep Aging Behavior of an Al-Mg-Si Alloy, Metall. Mater. Trans. A, 39 (2008) 243-251.

[6] C.S.T. Chang, J. Banhart, Low-Temperature Differential Scanning Calorimetry of an Al-Mg-Si Alloy, Metall. Mater. Trans. A, 42 (2011) 1960-1964.

[7] V. Fallah, B. Langelier, N. Ofori-Opoku, B. Raeisinia, N. Provatas, S. Esmaeili, Cluster evolution mechanisms during aging in Al–Mg–Si alloys, Acta Mater. 103 (2016) 290-300.

[8] L.P. Ding, Z.H. Jia, Z.Q. Zhang, R.E. Sanders, Q. Liu, G. Yang, The natural aging and precipitation hardening behaviour of Al-Mg-Si-Cu alloys with different Mg/Si ratios and Cu additions, Mater. Sci. Eng. A, 627 (2015) 119-126.

[9] C.D. Marioara, S.J. Andersen, T.N. Stene, H. Hasting, J. Walmsley, A.T.J. Van Helvoort, R. Holmestad, The effect of Cu on precipitation in Al–Mg–Si alloys, Philos. Mag. 87 (2007) 3385-3413.

[10] E.A. Mørtsell, C.D. Marioara, S.J. Andersen, J. Røyset, O. Reiso, R. Holmestad, Effects of Germanium, Copper, and Silver Substitutions on Hardness and Microstructure in Lean Al-Mg-Si Alloys, Metall. Mater. Trans. A, 46 (2015) 4369-4379.

[11] Y.Y. Weng, Z.H. Jia, L.P. Ding, Y.F. Pan, Y.Y. Liu, Q. Liu, Effect of Ag and Cu additions on natural aging and precipitation hardening behavior in Al-Mg-Si alloys, J. Alloys Compd. 695 (2017) 2444-2452.

[12] J. Buha, R.N. Lumley, A.G. Crosky, K. Hono, Secondary precipitation in an Al–Mg–Si–Cu alloy, Acta Mater. 55 (2007) 3015-3024.

[13] M.W. Zandbergen, A. Cerezo, G.D.W. Smith, Study of precipitation in Al–Mg–Si Alloys by atom probe tomography II. Influence of Cu additions, Acta Mater. 101 (2015) 149-158.

[14] V. Fallah, A. Korinek, N. Ofori-Opoku, B. Raeisinia, M. Gallerneault, N. Provatas, S. Esmaeili, Atomic-scale pathway of early-stage precipitation in Al–Mg–Si alloys, Acta Mater. 82 (2015) 457-467.

[15] A. de Vaucorbeil, W.J. Poole, C.W. Sinclair, The superposition of strengthening contributions in engineering alloys, Mater. Sci. Eng. A, 582 (2013) 147-154.

[16] R.K.W. Marceau, A. de Vaucorbeil, G. Sha, S.P. Ringer, W.J. Poole, Analysis of strengthening in AA6111 during the early stages of aging: Atom probe tomography and yield stress modelling, Acta Mater. 61 (2013) 7285-7303.

[17] M.J. Starink, N. Gao, L. Davin, J. Yan, A. Cerezo, Room temperature precipitation in quenched Al–Cu–Mg alloys: a model for the reaction kinetics and yield strength development, Philos. Mag. 85 (2005) 1395-1417.

[18] M.J. Starink, S.C. Wang, The thermodynamics of and strengthening due to co-clusters: General theory and application to the case of Al–Cu–Mg alloys, Acta Mater. 57 (2009) 2376-2389.

[19] A.J. Ardell, Precipitation Hardening, Metall. Trans. A 16 (1985) 2131-2165.

[20] S. CJ, Metals reference book. 7th ed, London: Butterworths-Heinemann, (1992).

[21] J.J. Wortman, R.A. Evans, Young's Modulus, Shear Modulus, and Poisson's Ratio in Silicon and Germanium, J. Appl. Phys. 36 (1965) 153.

[22] C. Wolverton, Solute–vacancy binding in aluminum, Acta Mater. 55 (2007) 5867-5872.

[23] S. Hirosawa, F. Nakamura, T. Sato, First-Principles Calculation of Interaction Energies between Solutes and/or Vacancies for Predicting Atomistic Behaviors of Microalloying Elements in Aluminum Alloys, Mater. Sci. Forum, 561-565 (2007) 283-286.

[24] P. Riveradiazdelcastillo, P. Reischig, S. Vanderzwaag, Tailoring of Ostwald ripening behaviour in multicomponent Al alloys, Scripta Mater. 52 (2005) 705-708.

Figure captions

Fig. 1. Vickers hardness for the four alloys (a) immediately after WQ and 2 weeks NA, (b) AA at 443 K for 5 min and 30 min immediately after WQ.

Fig. 2. Atoms maps for the four alloys after 2 weeks NA, (a) the A1 base alloy; (b) the Ag-added A2 alloy; (c) the Ag-Cu-added A3 alloy; (d) the Cu-added A4 alloy.

Fig. 3. Number density of clusters as a function of the cluster size for the four alloys after 2 weeks NA.

Fig. 4. Plots of the measured Mg/Si ratio of cluster against cluster size after 2 weeks NA for the four alloys, (a) the A1 base alloy; (b) the Ag-added A2 alloy; (c) the Ag-Cu-added A3 alloy; (d) the Cu-added A4 alloy.

Fig. 5. Plots of the measured X/Mg ratio against cluster size after 2 weeks NA treatment for the three Ag/Cu-added alloys, (a) the Ag-added A2 alloy; (b) the Ag-Cu-added A3 alloy; (c) the Cu-added A4 alloy.

Fig. 6. (a) Atoms maps for the four alloys after AA at 443 K for 5 min, (a) the A1 base alloy; (b) the Ag-added A2 alloy; (c) the Ag-Cu-added A3 alloy; (d) the Cu-added A4 alloy.

Fig. 7. Number density of particles as a function of the particle size for the four alloys after AA at 443 K for 5 min.

Fig. 8. Plots of the measured particle Mg/Si ratio against particle size after 5 min AA for the four alloys, (a) the A1 base alloy; (b) the Ag-added A2 alloy; (c) the Ag-Cu-added A3 alloy; (d) the Cu-added A4 alloy.

Fig. 9. Plots of the measured particle X/Mg ratio against particle size after 5 min AA treatment for the three Ag/Cu-added alloys, (a) the Ag-added A2 alloy; (b) the Ag-Cu-added A3 alloy; (c) the Cu-added A4 alloy.

Fig. 10. The schematic illustrations of cluster evolution in the A1 base alloy, the Ag-added A2 alloy and the Cu-added A4 alloy during NA treatment.

Fig. 11. The schematic illustrations of cluster evolution in the A1 base alloy, the Ag-added A2 alloy and the Cu-added A4 alloy during AA treatment.

Table captions

Table 1 Chemical compositions of the four alloys (at. %).

	Si	Mg	Fe	Mn	Ag	Cu
A1	0.68	1.21	0.05	0.03	-	-
A2	0.68	1.26	0.05	0.03	0.12	-
A3	0.68	1.27	0.05	0.03	0.07	0.10
A4	0.67	1.22	0.05	0.03	-	0.21

Table 2 Tensile results of the four alloys after NA and AA treatments

	2 weeks NA			**5 min AA**		
	YS (MPa)	**UTS** (MPa)	**Elongation** (%)	**YS**(MPa)	**UTS**(MPa)	**Elongation** (%)
A1	144.63	268.85	20.04	147.38	255.11	20.65
A2	163.44	285.58	18.98	210.84	318.23	18.68
A3	177.98	295.39	18.63	205.31	316.21	18.81
A4	186.84	300.63	18.21	185.48	306.89	19.41

Table 3 Compositions of clusters for the four alloys after 2 weeks NA obtained using a N_{min} of 10.

	Cluster Mg/Si ratio	**Cluster (Mg+X)/Si ratio**	**Cluster X/Mg ratio**
A1	1.89±0.03	—	—
A2	1.83±0.03	2.11±0.03	0.13±0.01
A3	1.48±0.02	1.62±0.02	0.03±0.01
A4	1.34±0.02	1.42±0.02	0.06±0.01

Table 4 Compositions of clusters and GP-zones for the four alloys after 5 min AA obtained using a N_{min} of 10.

	Cluster Mg/Si ratio	**Cluster (Mg+X)/Si ratio**	**Cluster X/Mg ratio**	**GP zone Mg/Si ratio**	**GP zone (Mg+X)/Si ratio**	**GP zone X/Mg ratio**

A1	1.67±0.03	—	—	2.29±0.03	—	—
A2	1.70±0.02	1.95±0.01	0.16±0.01	1.59±0.02	1.79±0.03	0.12±0.01
A3	1.65±0.03	1.84±0.03	0.14±0.01	1.59±0.02	1.75±0.02	0.10±0.01
A4	1.61±0.01	2.28±0.03	0.38±0.02	1.38±0.01	1.57±0.03	0.12±0.01

Table 5 Factors responsible to yield stress for the four alloy after 2 weeks NA.

Alloy	**Factor**	**Particle size (nm)**			
		0.4-0.6	**0.6-0.8**	**0.8-1.0**	**Total**
A1	μ (GPa)	24.34	23.64	—	—
	Volume frac (%)	0.0035	0.0030	—	0.0065
	$<r_g>$ (nm)	0.56	0.67	—	—
A2	μ (GPa)	23.82	24.18	24.45	—
	Volume frac (%)	0.0035	0.0026	0.0014	0.0075
	$<r_g>$ (nm)	0.56	0.65	0.88	—
A3	μ (GPa)	25.28	26.90	24.14	—
	Volume frac (%)	0.0032	0.0062	0.0022	0.0116
	$<r_g>$ (nm)	0.56	0.66	0.84	—
A4	μ (GPa)	24.69	24.92	24.33	—
	Volume frac (%)	0.0036	0.0072	0.0027	0.0135
	$<r_g>$ (nm)	0.55	0.65	0.95	—

Table 6 Factors responsible to yield stress for the four alloy after 5 min AA.

Alloy	**Factor**	**Particle size (nm)**						
		0.4-0.6	**0.6-0.8**	**0.8-1.0**	**1.0-1.2**	**1.2-1.4**	**1.4-1.6**	**Total**
A1	μ (GPa)	24.10	24.25	24.08	23.98	—	—	—
	Volume frac (%)	0.0139	0.0270	0.0142	0.0076	—	—	0.0627
	$<r_g>$ (nm)	0.55	0.68	0.87	1.09	—	—	—
A2	μ (GPa)	23.52	24.49	24.48	24.61	24.65	24.61	—
	Volume frac (%)	0.0414	0.1008	0.0655	0.0787	0.0588	0.0226	0.3678
	$<r_g>$ (nm)	0.55	0.68	0.89	1.09	1.30	1.87	—
A3	μ (GPa)	24.73	24.85	24.91	24.80	24.84	24.96	—
	Volume frac (%)	0.0400	0.0962	0.0670	0.0582	0.0546	0.0164	0.3324
	$<r_g>$ (nm)	0.55	0.68	0.88	1.09	1.28	1.46	—
A4	μ (GPa)	25.62	26.24	25.08	25.36	25.30	—	—
	Volume frac (%)	0.0231	0.0357	0.0229	0.0207	0.0105	—	0.1029
	$<r_g>$ (nm)	0.56	0.67	0.89	1.08	1.25	—	—

Table 7 Predicted yield stress ($\sigma_{particle}$, MPa) of different particles by modulus hardening for the four alloys.

Temper	**Alloy**	**Particle size (nm)**						
		$\sigma_{0.4\text{-}0.6}$	$\sigma_{0.6\text{-}0.8}$	$\sigma_{0.8\text{-}1.0}$	$\sigma_{1.0\text{-}1.2}$	$\sigma_{1.2\text{-}1.4}$	$\sigma_{1.4\text{-}1.6}$	**Total$_\sigma$**
NA for 2 weeks	**A1**	5.55	2.80	—	—	—	—	**8.35**
	A2	5.39	2.74	0.35	—	—	—	**8.48**
	A3	5.46	4.63	0.45	—	—	—	**10.55**

	A4	5.79	4.71	0.44	—	—	—	**10.95**
443 K AA for 5 minutes	**A1**	11.12	8.46	1.11	0.44	—	—	**21.12**
	A2	18.76	16.52	2.36	1.44	5.37	5.58	**50.03**
	A3	19.38	16.37	2.45	1.25	5.29	4.76	**49.51**
	A4	15.00	10.69	1.43	0.77	2.42	—	**30.30**

Table 8 Diffusion data and diffusion coefficient D for studied solute atoms at 293 K and 443 K.

Diffuser	**D_0 (m^2/s)**	**Q (KJ/mole)**	**$D_{293}\times10^{26}$ (m^2/s)**	**$D_{443}\times10^{20}$ (m^2/s)**
Mg	1.49×10^{-5}	120.5	0.478	9.07
Si	1.38×10^{-5}	117.6	1.46	18.5
Cu	4.44×10^{-5}	133.9	5.82×10^{-3}	0.71
Ag	1.30×10^{-5}	117.0	1.76	20.4

Table 9 Interaction energies (in eV) between solute atoms in Al-Mg-Si alloys through a first-principles calculation.

	Mg	**Si**	**Ag**	**Cu**	**$V_{vacancy}$**
Mg	0.0387	-0.0422	-0.0632	-0.0409	-0.0144
Si		0.0262	0.0437	0.0388	-0.0242
Ag			-0.0768	-0.0460	-0.0865
Cu				0.0216	0.0499
$V_{vacancy}$					0.0645

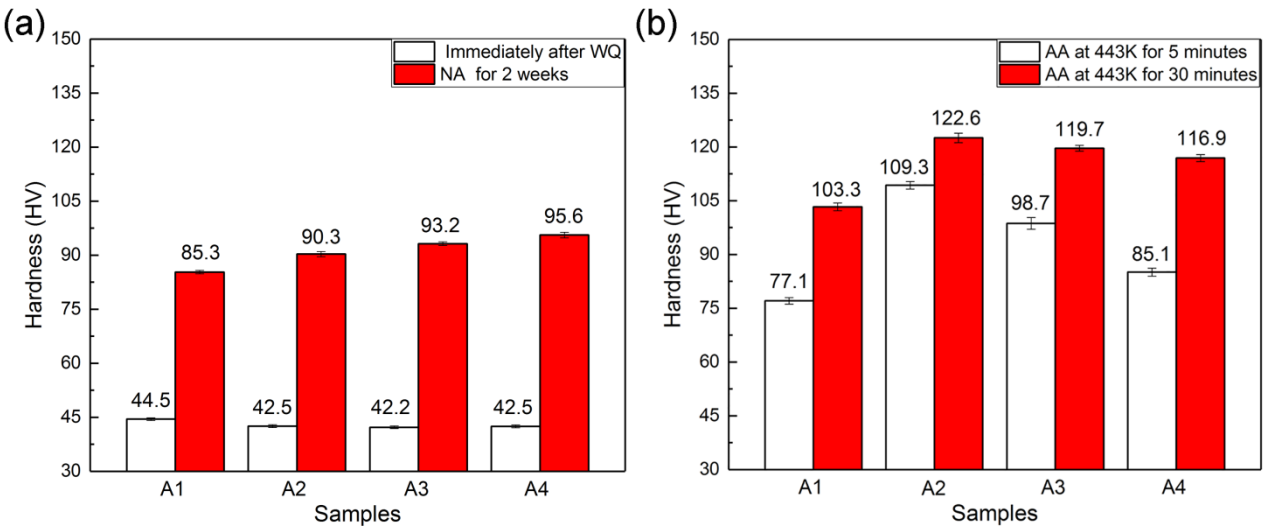

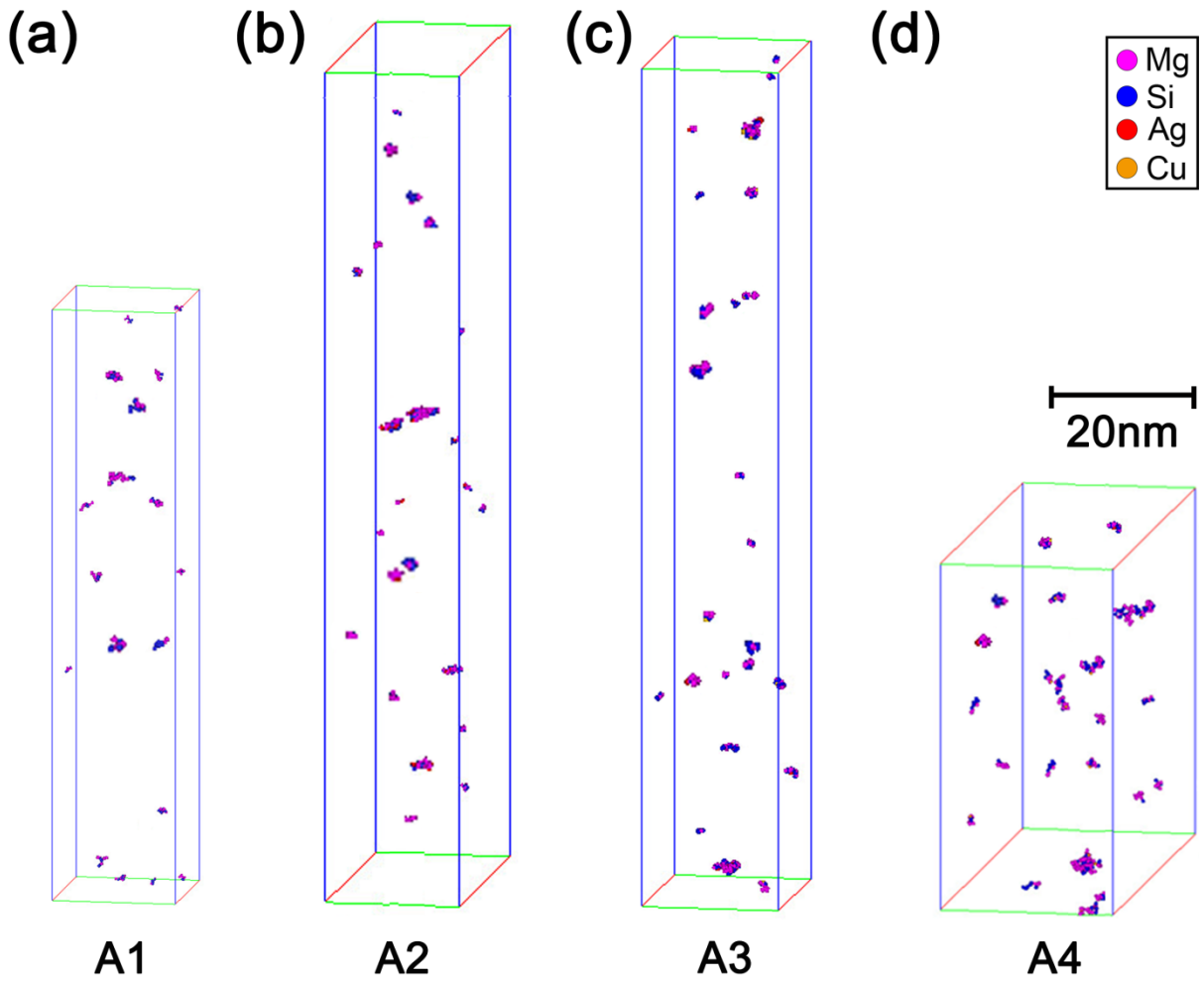

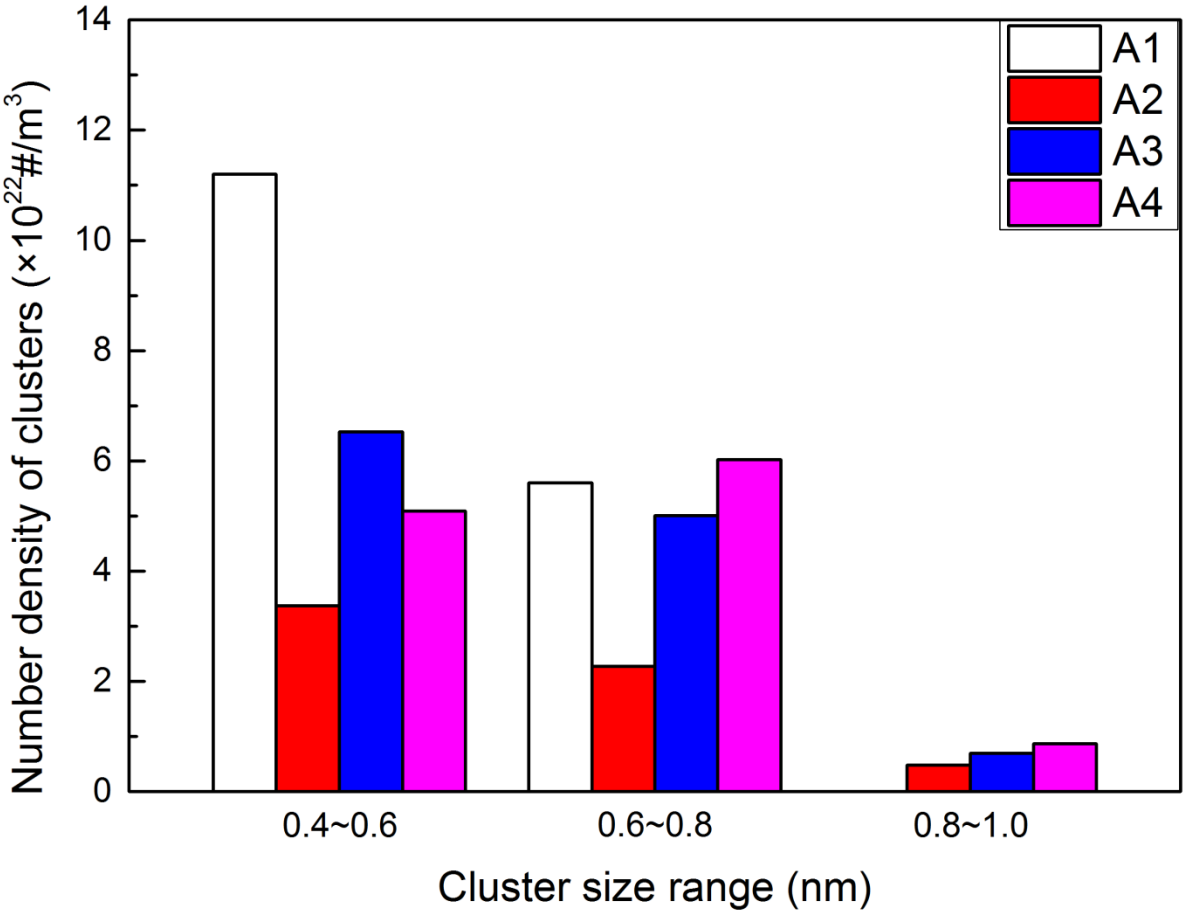

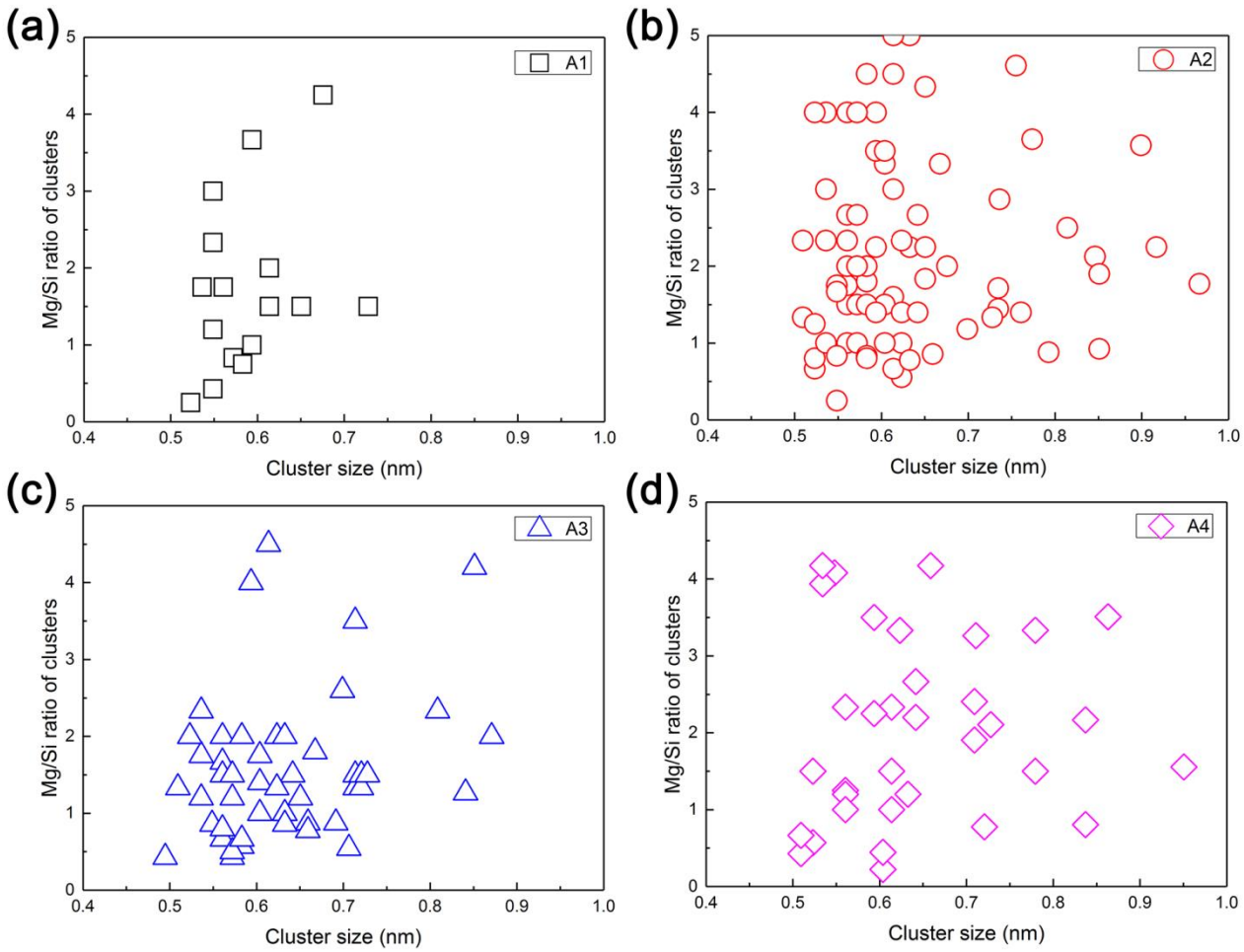

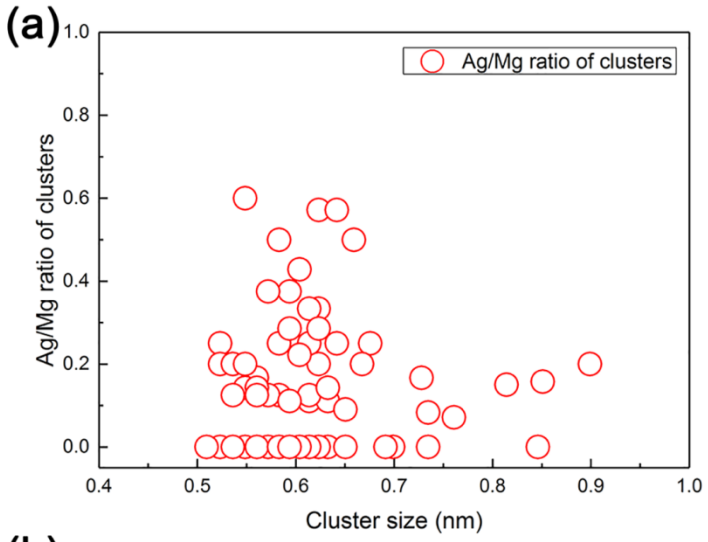

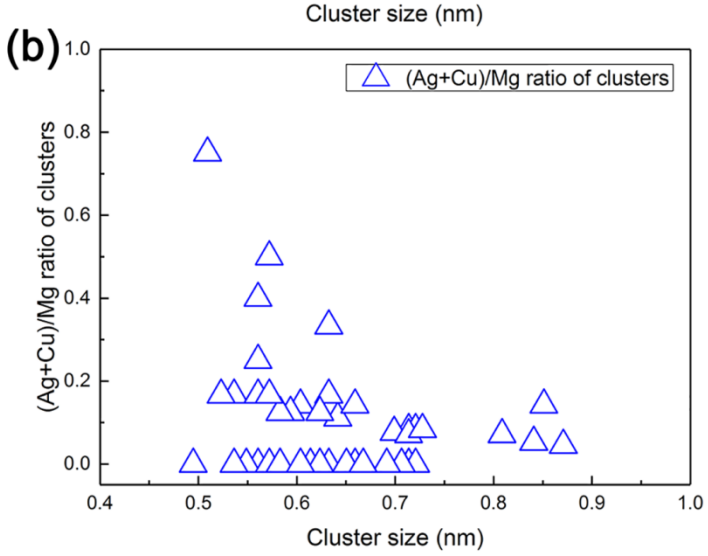

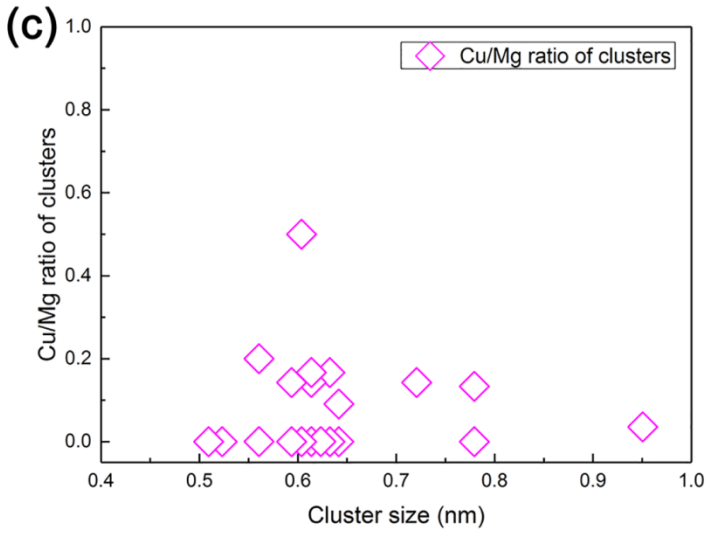

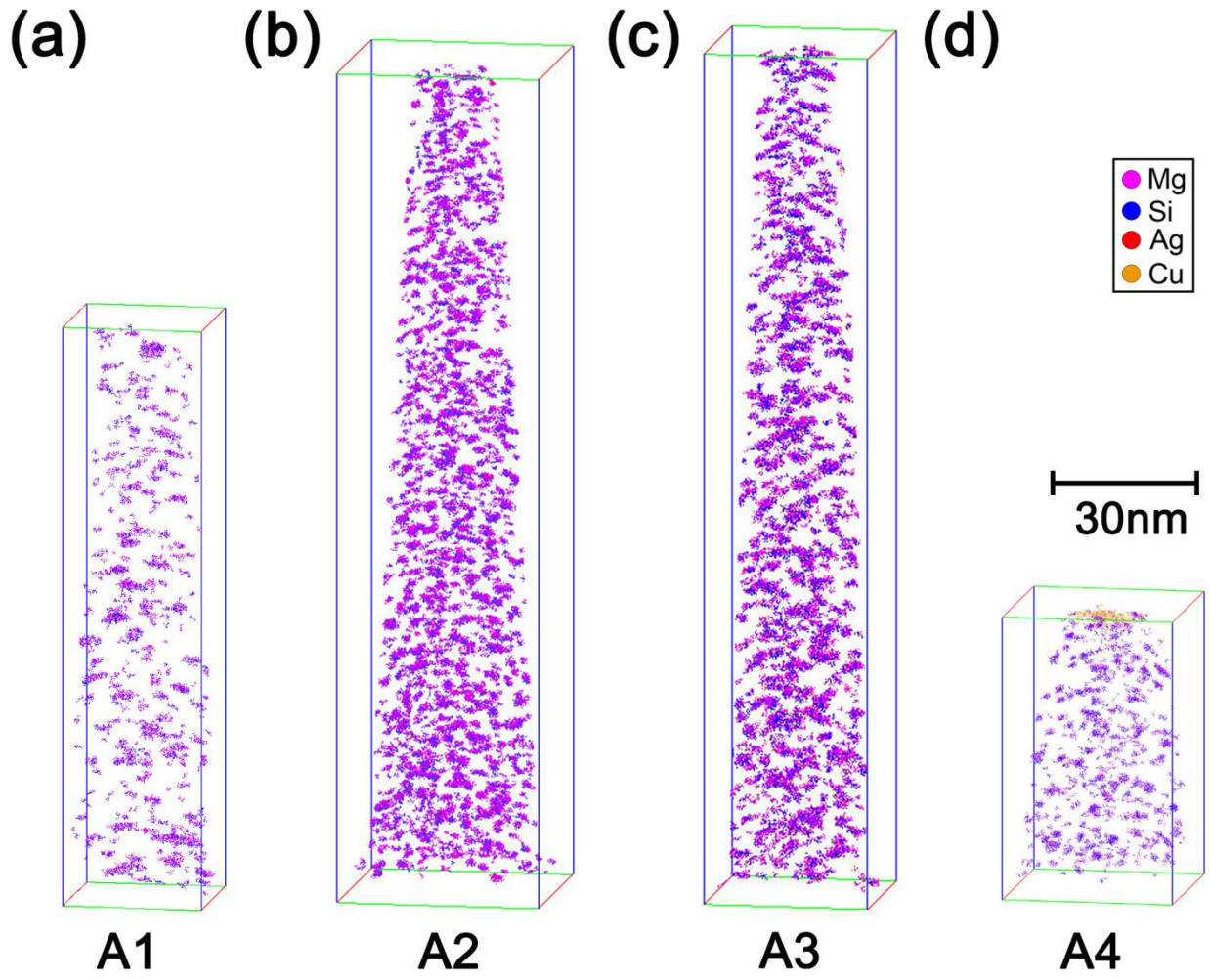

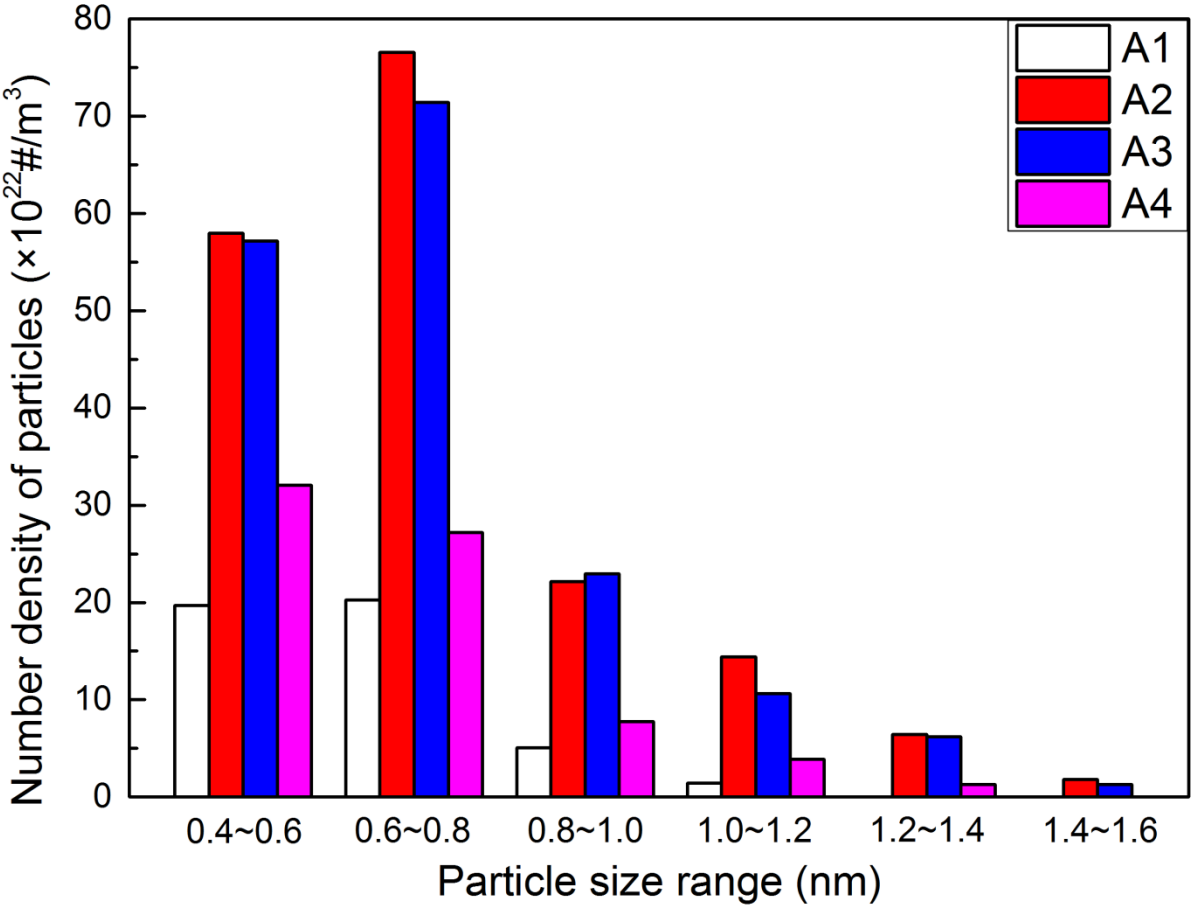

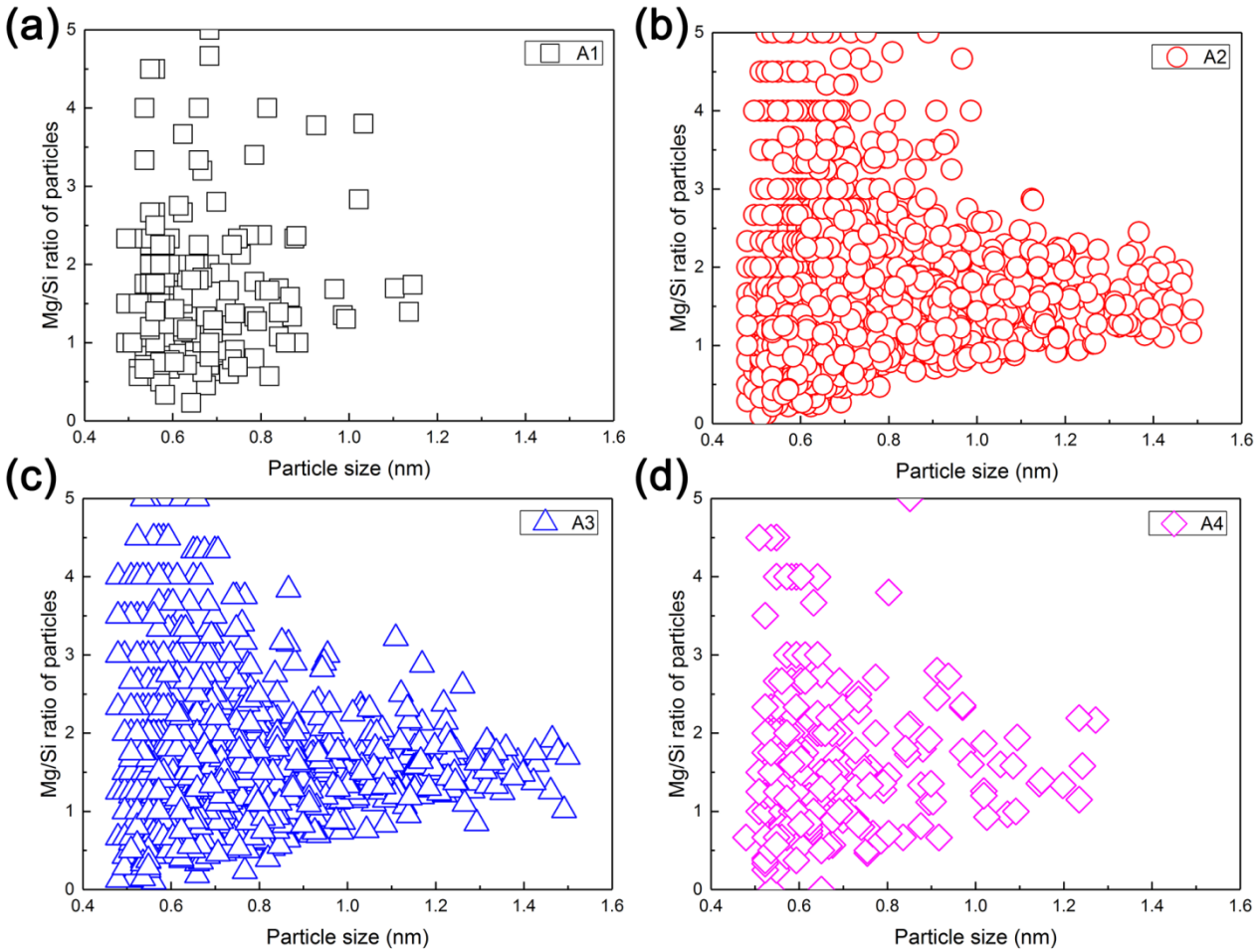

(a)

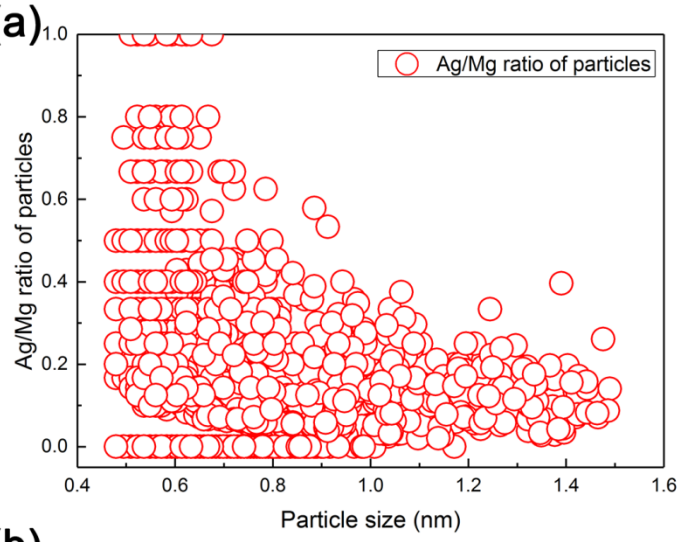

(b)

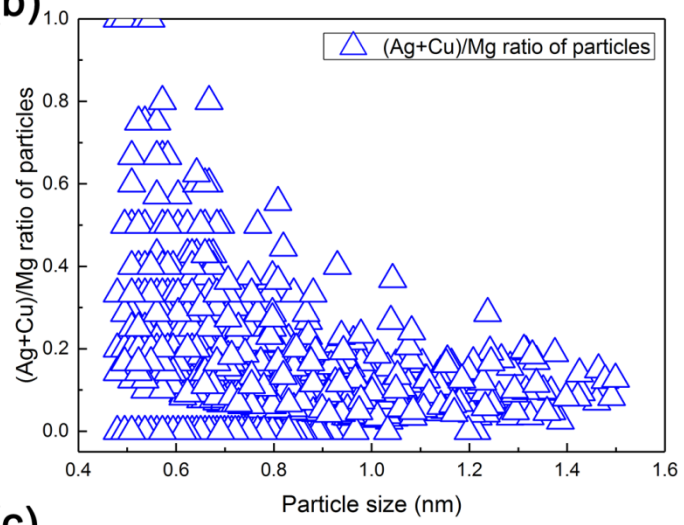

(c)